Accepted Manuscript

A multidisciplinary study of 3-(β-D-glucopyranosyl)-5-substituted-1,2,4-triazole derivatives as glycogen phosphorylase inhibitors: Computation, synthesis, crystallography and kinetics reveal new potent inhibitors

Sándor Kun, Jaida Begum, Efthimios Kyriakis, Evgenia C.V. Stamati, Thomas A. Barkas, Eszter Szennyes, Éva Bokor, Katalin E. Szabó, George A. Stravodimos, Ádám Sipos, Tibor Docsa, Pál Gergely, Colin Moffatt, Myrto S. Patraskaki, Maria C. Kokolaki, Alkistis Gkerdi, Vassiliki T. Skamnaki, Demetres D. Leonidas, László Somsák, Joseph M. Hayes

PII: S0223-5234(18)30117-X

DOI: 10.1016/j.ejmech.2018.01.095

Reference: EJMECH 10172

To appear in: *European Journal of Medicinal Chemistry*

Received Date: 28 December 2017

Revised Date: 26 January 2018

Accepted Date: 30 January 2018

Please cite this article as: Sá. Kun, J. Begum, E. Kyriakis, E.C.V. Stamati, T.A. Barkas, E. Szennyes, É. Bokor, K.E. Szabó, G.A. Stravodimos, Áá. Sipos, T. Docsa, Pá. Gergely, C. Moffatt, M.S. Patraskaki, M.C. Kokolaki, A. Gkerdi, V.T. Skamnaki, D.D. Leonidas, Láó. Somsák, J.M. Hayes, A multidisciplinary study of 3-(β-D-glucopyranosyl)-5-substituted-1,2,4-triazole derivatives as glycogen phosphorylase inhibitors: Computation, synthesis, crystallography and kinetics reveal new potent inhibitors, *European Journal of Medicinal Chemistry* (2018), doi: 10.1016/j.ejmech.2018.01.095.

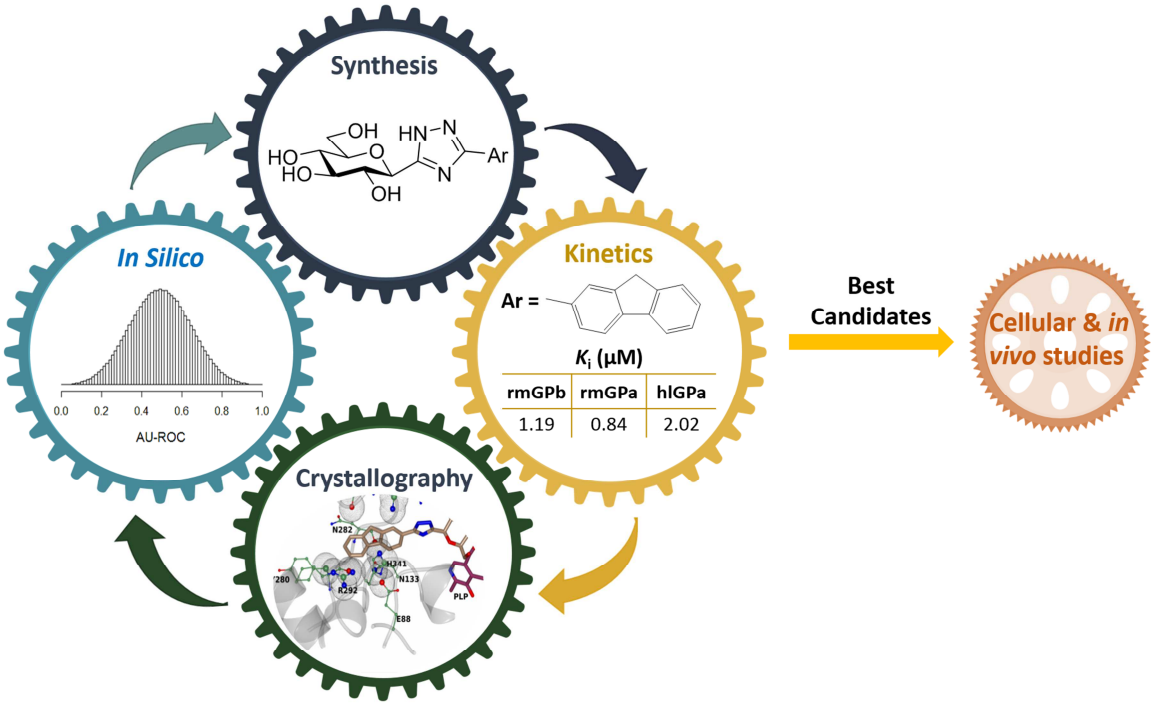

A multidisciplinary study of 3-(β-D-glucopyranosyl)-5-substituted-1,2,4-triazole derivatives as glycogen phosphorylase inhibitors: computation, synthesis, crystallography and kinetics reveal new potent inhibitors

Sándor Kun,[a#] Jaida Begum,[b,c#] Efthimios Kyriakis,[d#] Evgenia C.V. Stamati,[d] Thomas A. Barkas,[d] Eszter Szennyes,[a] Éva Bokor,[a] Katalin E. Szabó,[a] George A. Stravodimos,[d] Ádám Sipos,[e] Tibor Docsa,[e] Pál Gergely,[e] Colin Moffatt,[f] Myrto S. Patraskaki,[d] Maria C. Kokolaki,[d] Alkistis Gkerdi,[d] Vassiliki T. Skamnaki,[d] Demetres D. Leonidas,*[d] László Somsák,*[a] Joseph M. Hayes*[b]

[a] *Department of Organic Chemistry, University of Debrecen, POB 400, H-4002 Debrecen, Hungary*

[b] *School of Physical Sciences & Computing, Division of Chemistry, University of Central Lancashire, Preston PR1 2HE, United Kingdom*

[c] *School of Chemistry, University of Leeds, Leeds, LS2 9JT, United Kingdom*

[d] *Department of Biochemistry & Biotechnology, University of Thessaly, Biopolis, 41500 Larissa, Greece*

[e] *Department of Medical Chemistry, Faculty of Medicine, University of Debrecen, Egyetem tér 1, H-4032 Debrecen, Hungary*

[f] *Health and Life Sciences, De Montfort University, Gateway House, Leicester. LE1 9BH, United Kingdom*

[*] Corresponding authors
tel: +302410565278 (DDL); fax: +302410565291; email: ddleonidas@bio.uth.gr
tel: +3652512900 ext 22348 (LS); fax: +3652512744; e-mail: somsak.laszlo@science.unideb.hu
tel: +441772894334 (JMH); fax: +441772894981; email: jhayes@uclan.ac.uk
[#]Equal contribution

Abstract: 3-(β-D-Glucopyranosyl)-5-substituted-1,2,4-triazoles have been revealed as an effective scaffold for the development of potent glycogen phosphorylase (GP) inhibitors but with the potency very sensitive to the nature of the alkyl/aryl 5-substituent (Kun *et al.*, Eur. J. Med. Chem. 2014, 76, 567). For a training set of these ligands, quantum mechanics-polarized ligand docking (QM-PLD) demonstrated good potential to identify larger differences in potencies (predictive index PI = 0.82) and potent inhibitors with K_i's < 10 μM (AU-ROC = 0.86). Accordingly, *in silico* screening of 2335 new analogues exploiting the ZINC docking database was performed and nine predicted candidates selected for synthesis. The compounds were prepared in *O*-perbenzoylated forms by either ring transformation of 5-β-D-glucopyranosyl tetrazole by *N*-benzyl-arenecarboximidoyl chlorides, ring closure of *C*-(β-D-glucopyranosyl)formamidrazone with aroyl chlorides, or that of *N*-(β-D-glucopyranosylcarbonyl)arenethiocarboxamides by hydrazine, followed by deprotections. Kinetics experiments against rabbit muscle GPb (rmGPb) and human liver GPa (hlGPa) revealed five compounds as potent low μM inhibitors with three of these on the submicromolar range for rmGPa. X-ray crystallographic analysis sourced the potency to a combination of favorable interactions from the 1,2,4-triazole and suitable aryl substituents in the GP catalytic site. The compounds also revealed promising calculated pharmacokinetic profiles.

Keywords: 1,2,4-triazole, *C*-β-D-glucopyranosyl derivatives, glycogen phosphorylase inhibitors, QM/MM docking, kinetics, X-ray crystallography

1. Introduction

Type 2 diabetes (T2D) is a heterogeneous disease characterized by hyperglycemia. The incidence of diabetes is on the rise globally with approximately 422 million people currently affected and with ~90% of these cases T2D [1]. Current approaches to management of T2D include modifications to diet, regular exercise and prescribed oral antihyperglyaemic drugs. Adequate control of blood glucose levels is crucial to reduce the incidence of the long term complications of T2D such as nephropathy, neuropathy and an increased risk of blindness and cardiovascular disease [2]. However, current antihyperglycaemic drugs have somewhat limited efficacy in this regard.

Glycogen phosphorylase (GP; EC 2.4.1.1) is a validated target for the development of new T2D treatments having a direct influence on blood glucose levels through the glycogenolysis pathway [3]. Structurally, GP exists as a homodimer consisting of two identical subunits, each 842 residues long. It is regulated allosterically by phosphorylation, has pyridoxal-5-phosphate (PLP) as co-factor, and exists in two interconvertible forms: the phosphorylated predominantly active R state (GPa), and the unphosphorylated predominantly inactive T state (GPb). Seven different GP binding sites have been identified to date offering multiple opportunities for modulation of enzymatic activity [4-6]: the catalytic, allosteric, new allosteric, inhibitor, glycogen storage, benzimidazole [7] and quercetin binding site [8]. A large number of synthetic and natural product GP inhibitors targeting the different binding sites have been identified in recent years and solved structures of inhibitor bound GP complexes have facilitated further structure based inhibitor design efforts [4, 5, 9]. GP inhibitors have demonstrated considerable potential for T2D treatment in cellular models [10-12] and *in vivo* [13-16], as well as promise against other conditions such as myocardial and cerebral ischemias, and tumors [17-19].

Of the different GP binding sites, the catalytic site has been explored most in terms of inhibitor design efforts. The physiological inhibitor of GP is α-D-glucose (K_i = 1.7 mM) and rational design of α and β-substitutions at the anomeric carbon have proved effective towards increasing inhibitor potency [4, 5, 9, 20, 21]. β-Substitutions have proved particularly effective by exploiting favorable interactions in the so-called β-cavity of the catalytic site, a pocket lined by both polar and non-polar residues. Choice of the linker group which connects the glucose moiety with different alkyl/aryl substituents is critical to inhibitor potency [4]. Among recently reported potent catalytic site inhibitors [22, 23], *C*-glucopyranosyl-1,2,4-triazoles have been revealed as a novel scaffold (Table 1) for the design of potent GP inhibitors [23, 24] with **I** and **II** exhibiting potencies of 0.41 and 0.67 μM, respectively. The potencies, however, are very sensitive to the alkyl/aryl ligand substituent occupying the β-cavity, with 50% of the compounds reported to date (**X-XVIII**) having K_i's > 100 μM to no inhibition.

With this in mind, we report here the exploitation of the *C*-glucopyranosyl-1,2,4-triazole skeleton (Table 1) for the design of new potent GP inhibitors. Using the previously reported compounds with known inhibition constants (K_i's) as a training set (Table 1) [23, 24], we have investigated different docking methods to reproduce the trends in binding affinities for this congeneric series of compounds. Quantum mechanics/molecular mechanics (QM/MM) docking in the form of quantum mechanics – polarised ligand docking (QM-PLD) with Glide and QSite [25] was found to perform best as determined by a rigorous statistical analysis. Then, exploiting the ZINC docking database (http://zinc.docking.org/) [26], different –R groups (with a basic substructure phenyl) from commercially available acids, acid chlorides and aldehydes led to the virtual screening of 2335 new *C*-glucopyranosyl-1,2,4-triazole

analogues. Nine of the screened candidates were selected for synthesis and extensive kinetics studies performed. Five of the nine candidates revealed potencies better than the threshold employed for 'activity' (K_i < 10 μM) with three compounds in the upper-nanomolar range for rmGPa. These inhibitors are among the most potent catalytic site inhibitors discovered to date. Crystallographic studies have been performed and these structural studies have revealed the interactions that govern the observed potencies. Favorable pharmacokinetic profiles are critical to the effectiveness of these inhibitors at the cellular level and *in vivo*. In this regard, absorption, distribution, metabolism and excretion (ADME) predictions are additionally reported and analyzed.

Table 1. Training set of 3-(*β*-D-glucopyranosyl)-5-substituted-1,2,4-triazoles with their inhibition data towards rmGPb.[23]

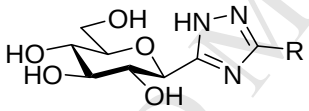

	R	K_i [μM]		R	K_i [μM]
I	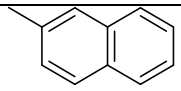	0.41	**X**	$-CH_2OH$	105
II	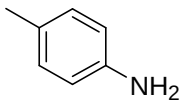	0.67	**XI**	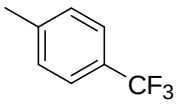	111
III	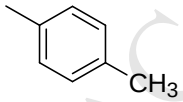	1.7	**XII**	$-CH_3$	499
IV	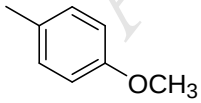	1.9	**XIII**	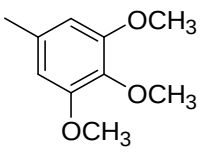	518*
V	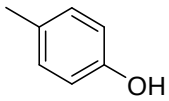	2.9	**XIV**	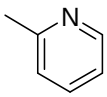	707

VI	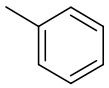	7	**XV**	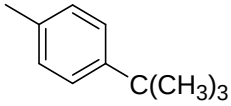	778
VII	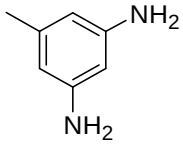	14	**XVI**	$-C(CH_3)_3$	no inh. at 625 µM
VIII	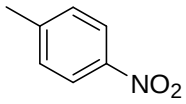	33.5	**XVII**	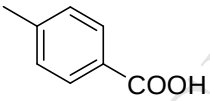	no inh. at 625 µM
IX	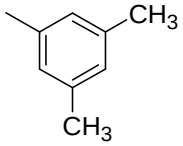	39.7	**XVIII**	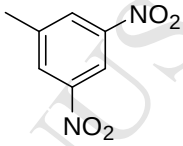	no inh. at 625 µM

*Calculated from the IC_{50} value by using a web-based tool.[27]

2. Results & Discussion

2.1 *In Silico* Selection of Synthetic Candidates

2.1.1 Training Set Results

The training set of 3-(*β*-D-glucopyranosyl)-5-substituted-1,2,4-triazoles used in this study represent a congeneric series of 18 compounds (Table 1) with a good spread of K_i values ranging from 0.41 µM to no inhibition [23, 24]. 'Activity' was defined in terms of inhibitor potency throughout. Performance of different docking methods, Glide-SP (standard-precision), -XP (extra-precision) and QM-PLD with respect to the prediction of ligand activities was analyzed in a statistical manner. The correlation between predicted and experimental activities was measured using the Pearson (R_P) and Spearman (R_S) correlation coefficients, which quantify the relative strength (and direction) of a relationship. Rp is parametric and takes into account the absolute differences between experimental data (binding

free energies) and predictions (docking score); R_S describes the non-parametric relationship between the activity ranks of the ligands in the two datasets. Rp is a better measure for absolute predictions (binding affinities), with R_S more appropriate for relative ranking[28, 29] and therefore assumes priority over Rp in this work. Additionally, we considered the 'predictive index' (PI) [30]. This metric provides an important additional measure for the relative ranking of ligand potencies by using a weight that depends on the difference between the experimental activities of ligands. Therefore, the PI reflects that a good model should be able to differentiate ligands which have larger differences in potencies, whereas if potencies are similar, the weight will be low. PI values range from -1 (predictions always wrong) to +1 (predictions always right), with 0 corresponding to predictions that are completely random. Finally, the area under the ROC (AU-ROC) curve metric was calculated for each docking model representing the probability of active compounds being ranked earlier than inactive compounds (range 0-1). For AU-ROC, we used a threshold of K_i < 10 µM to define activity, leading to n = 6 actives in the set of N = 18 compounds. While a smaller dataset alters the shape of the null distributions (Figure 1), it does not limit its application to studies of this type, which has also included the CSAR benchmark exercises [29]. The statistical metrics used in our analysis are described in more detail in the Supplementary Information.

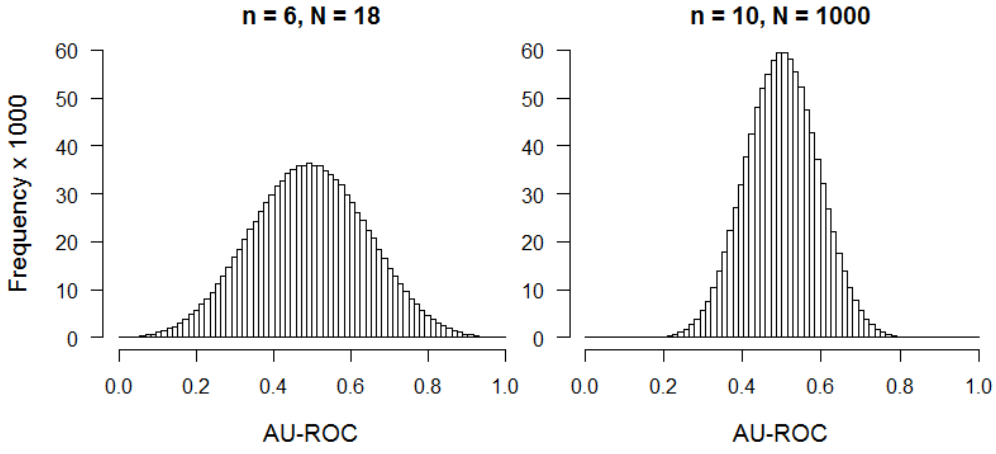

Figure 1. Comparison of AU-ROC null distributions for a set of n = 6 actives in a set of 18 ligands (this study) versus a representative set of n = 10 actives in a set of 1000 ligands used in larger scale virtual screening. Distributions were created by random selection of ligands and calculation of AU-ROC for each of these selections using the program R [31]. With a smaller pool of ligands, random selection of the best or worst subset is more likely, hence the wider and shorter distribution on the left. Statistically significant models, however, will still be indicated by p-values < 0.05.

The results for statistical analysis of docking performance are shown in Table 2. Improvement of results with increasing 'accuracy' of the docking algorithms was observed from Glide-SP (Rp = 0.59, R_S = 0.65, PI = 0.70) to –XP (Rp = 0.73, R_S = 0.73, PI = 0.77). A high AU-ROC value of 0.89 for Glide-XP was obtained indicating the efficiency of the algorithm to recognize inhibitors with K_i's less than the 10 μM threshold value. Superior performance of QM/MM docking approaches has previously been reported [32-35], including for the GP catalytic site [34]. QM-PLD involved reparametrization of the ligand atomic charges in the field of the receptor using single point QM/MM calculations, with the ligand representing the QM region and described using B3LYP/LACVP* [36-40]. Using these new electrostatic potential (ESP) fit ligand charges, ligands were redocked using Glide-XP. For QM-PLD, while the Rp (0.71) and AU-ROC (0.86) values were similar to those from Glide-XP, metrics reflecting performance with respect to relative ranking of activities were improved for QM-PLD (R_S = 0.77, P.I. = 0.82). A PI value of 0.82 is comparable to a PI value of 0.84 obtained for a congeneric series of 16 p38 MAP kinase protein using computationally expensive thermodynamic integration (TI) free energy simulations [30]. Overall, while QM-PLD did produce reasonable correlation between predicted and experimental values for scores and affinity, respectively (Pearson Rp = 0.71), and relative ranking of potencies (Spearman Rs = 0.77), it demonstrated better potential to identify larger differences in potencies (predictive index PI = 0.82) and potent inhibitors with K_i's < 10 μM (AU-ROC = 0.86). This suggested the potential of QM-PLD to correctly propose potent 3-(*β*-D-glucopyranosyl)-5-substituted-1,2,4-triazole analogues at the screening stage. Probabilities (*p*-values) which reflect the

robustness of the predictions were all << 0.05 (Table 2) and validate their statistical significance.

Table 2. For the training set of eighteen 3-(*β*-D-glucopyranosyl)-5-substituted-1,2,4-triazoles (Table 1), statistical analysis of the agreement between docking and experimental activities as described in the text.[a]

	Pearson Correlation			Spearman Correlation						
Method	R_P	p-value	t-value	R_S	p-value	t-value	PI	p-value	AU-ROC	p-value
Glide-SP	0.59	0.020	2.64	0.65	0.008	3.11	0.70	0.0029	0.76	0.0352
Glide-XP	**0.73**	**0.002**	**3.83**	0.73	0.003	3.80	0.77	0.0007	**0.89**	**0.0035**
QM-PLD	0.71	0.003	3.64	**0.77**	**0.001**	**4.37**	**0.82**	**0.0002**	0.86	0.0064

[a] The best values for each metric are highlighted in bold. For the correlation coefficients R_p and R_s, p-values are derived from the t-distribution (t-values) for n - 2 degrees of freedom (13).

2.1.2 Screening Set Results

Based on the training set results, virtual screening of 2335 new 3-(*β*-D-glucopyranosyl)-5-substituted-1,2,4-triazoles was performed using QM-PLD. As all training set ligands were predicted to preferentially bind in one tautomeric state of the 1,2,4-triazole (tautomer shown in Table 1) forming hydrogen bond interactions with His377 O, only this tautomeric state was considered in the calculations. This favorable interaction was later confirmed in our crystallographic studies (*vide infra*). Nine candidates (target compounds **10a-f** and **10h-j** as per Scheme 1 and Table 3) were selected for synthesis based on the novelty of their chemical structure, docking scores, predicted interactions with GPb, synthetic viability and commercial availability of starting materials. **10g** was not screened but was of academic interest.

2.2 Syntheses

The target compounds were prepared by adapting our methods for the synthesis of *C*-glucopyranosyl 1,2,4-triazoles (Scheme 1) [23, 24, 41-43]. Synthetic studies were started by transformations of tetrazole **1** [44] since this method proved to be the most versatile one in previous investigations (Route A) [23]. Thus, *N*-benzyl arenecarboxamides **5** were treated

with $SOCl_2$ to give imidoyl chlorides which, without isolation and purification, were reacted with **1** in boiling xylene to result in the corresponding fully protected 1,2,4-triazole derivatives **6aa**, **ba**, and **c-e**. Removal of the benzyl protecting groups by catalytic hydrogenation furnished **7a-d** which were further deprotected to **10a-d** by the Zemplén protocol. Protective group cleavage of **6d** and **6e** was also effected in a reversed order to give **9d** and **9e** under Zemplén conditions. Catalytic hydrogenolysis of **9e** yielded **10e**, however, *N*-benzyl cleavage failed from **9d** even at higher temperature and pressure in a sealed tube. In order to get the sulfamoylated derivatives **10f** and **g**, tosyl amidrazone **2** was acylated [24, 43] by 4-sulfamoylbenzoyl chlorides to **7f** and **g** which, on Zemplén transesterification, produced **10f** and **g**, respectively (Route B). None of these methods proved suitable to prepare triazoles **7h-j** which could, however, be obtained via Route C [42]. Thus, anhydro-aldonic acid **3** was converted to the corresponding acid chloride **4** [45] which was reacted with thioamides to give the *N*-(β-D-glucopyranosylcarbonyl)thioamides **8h-j**. Ring closure of compounds **8** by hydrazine hydrate furnished 1,2,4-triazoles **7h-j** which were then *O*-debenzoylated by the Zemplén method to the target compounds **10h-j**.

Scheme 1. Synthesis of the target *C*-glucopyranosyl 1,2,4-triazoles **10**.

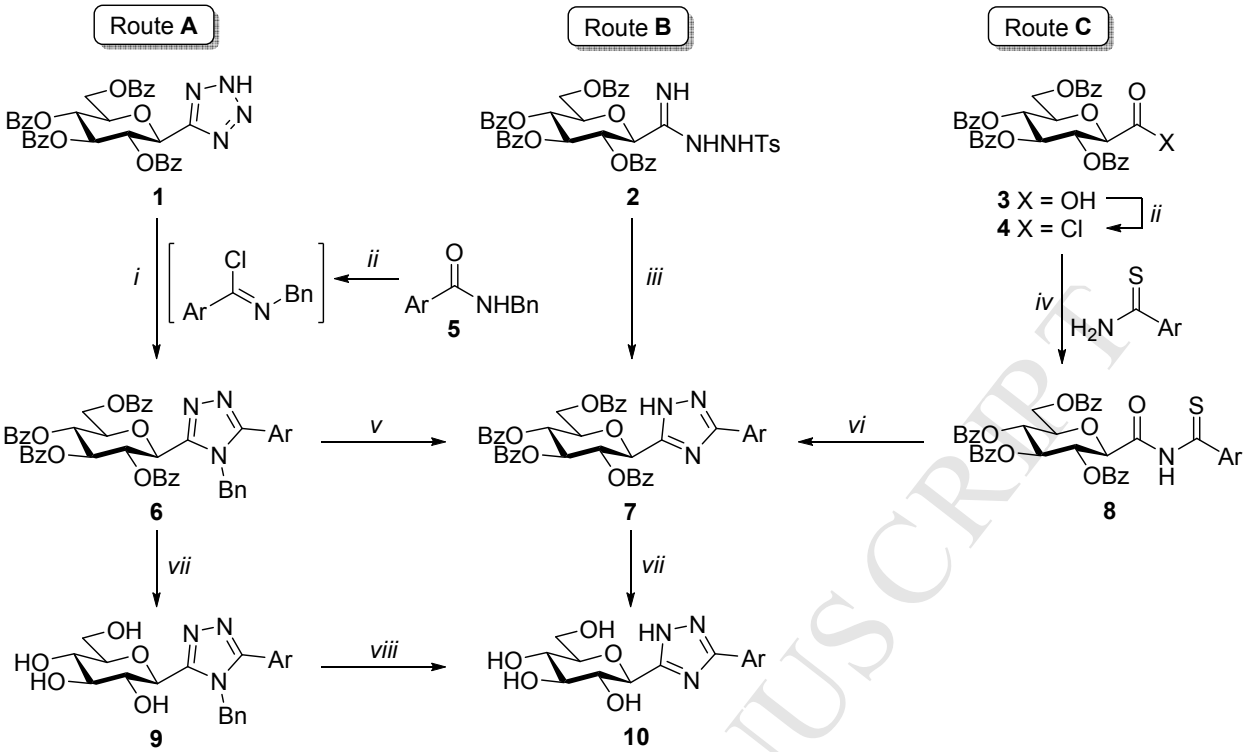

Reagents and conditions: *i*) anhydr. *m*-xylene at boiling temp.; *ii*) $SOCl_2$ at boiling temp.; *iii*) 1. ArCOCl, anhydr. $CHCl_3$, pyridine 0 °C → rt, 2. Bu_4NF, THF at boiling temp.; *iv*) anhydr. CH_3CN, pyridine, rt; *v*) H_2 (1 atm), Pd(C), anhydr. EtOAc or THF, both at boiling temp.; *vi*) $NH_2NH_2 \cdot H_2O$, pyridine, rt; *vii*) cat. NaOMe, anhydr. MeOH, $CHCl_3$, rt; *viii*) H_2 (1 atm), Pd(C), anhydr. MeOH, EtOAc at boiling temp.

Table 3: Structure of the aromatic moieties (Ar) for the compounds in Scheme 1 and the corresponding yields of the reactions.

Ar		Route	Isolated yield				
			6	**7**	**8**	**9**	**10**
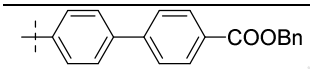	**aa**	A	63	-	-	-	-
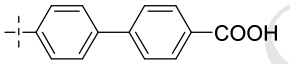	**a**	A	-	62	-	-	76
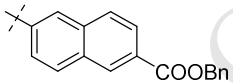	**ba**	A	64	-	-	-	-
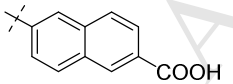	**b**	A	-	77	-	-	77
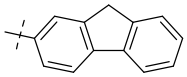	**c**	A	37	86	-	-	52
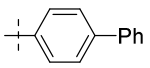	**d**	A	64	60	-	97	94 (from **7**)
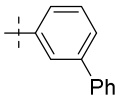	**e**	A	46	-	-	81	81
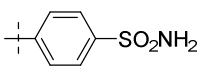	**f**	B	-	47	-	-	75

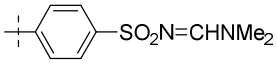	**g**	B	-	42	-	-	56
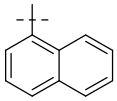	**h**	C	-	70	71	-	90
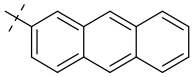	**i**	C	-	65	58	-	70
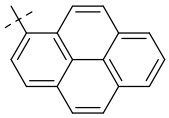	**j**	C	-	74	81	-	90

2.3 Enzyme Kinetics

The inhibition constant value (K_i) of the synthesized compounds for human liver glycogen phosphorylase *a* (hlGP*a*) together with the values for rmGPa (to compare the effect of the compounds in the liver and muscle) and rmGPb (to validate structural data) are summarized in Table 4. As the data shows for rmGPb, inhibitors **10a-d** are almost equipotent (K_i's 1.19 – 5.05 μM) while **10h** is somewhat less potent (K_i = 11.50 μM) and close to our threshold value for 'activity' (K_i < 10 μM). Compounds **10e**, **10f** and **10i** are moderate inhibitors (K_i's 20 – 98.2 μM) while **10j** and **10g** do not show any significant inhibition. However, there were some solubility issues for **10j**, while **10g** was not one of our predicted compound. From the K_i values it seems that completely non-polar substituents like fluorene (**10c**) or biphenyl (**10d**) increase the potency more than more polar ones like carboxy-biphenyl (**10a**) and carboxy-naphthyl (**10b**), or at least the effect of the polar carboxylate groups on potency is neutral. Of significant interest is the fact that the change of the position of the second phenyl ring at the biphenyl substituent from the meta position (**10e**) to the para (**10d**) leads to an approximately 28-fold increase in potency. Compounds **10a** (K_i = 0.98 μM), **10b** (K_i = 0.78 μM) and **10c** (K_i = 0.84 μM) show a preference for rmGPa with sub-micromolar activity observed, while **10d** displays similar potency for all three enzymes.

Table 4. Inhibition of glycogen phosphorylases by the synthesized compounds and crystallographic numbering.

Code	Compounds	K_i (μM)		
		rmGPb	rmGPa	hlGPa
10a	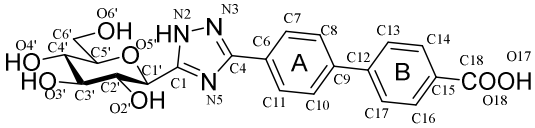	4.42 ± 0.17	0.98 ± 0.04	2.67 ± 0.12
10b	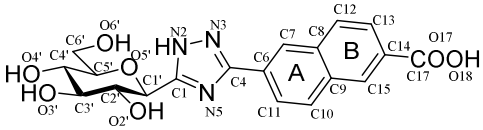	5.05 ± 0.40	0.78 ± 0.05	3.88 ± 0.13
10c	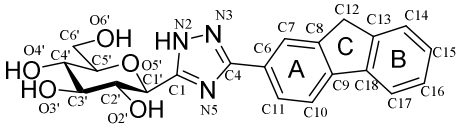	1.19 ± 0.13	0.84 ± 0.07	2.02 ± 0.33
10d	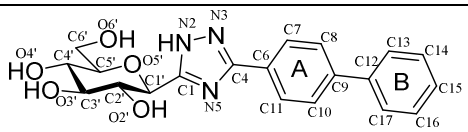	2.38 ± 0.19	2.09 ± 0.18	2.23 ± 0.08
10e	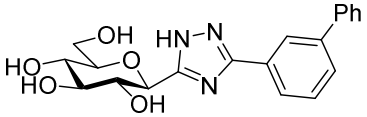	68.2[a]	N. m.[b]	N. m.[b]
10f	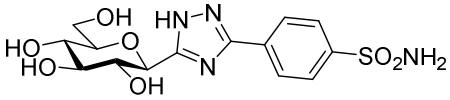	98.2[a]	N. m.[b]	N. m.[b]
10g	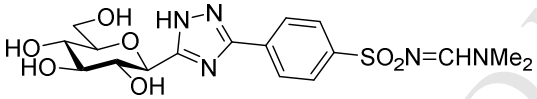	no inh. at 625 μM	N. m.[b]	N. m.[b]
10h	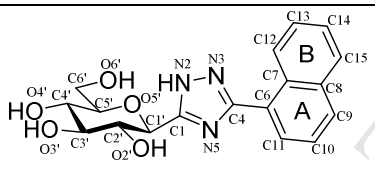	11.50 ± 0.23	3.38 ± 0.28	8.91 ± 0.44
10i	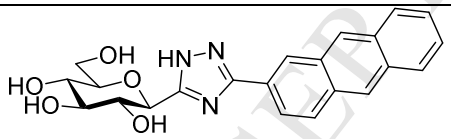	20 ± 0.95	N. m.[b]	N. m.[b]
10j	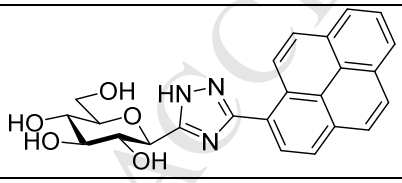	>1.5 mM	N. m.[b]	N. m.[b]

[a] Calculated from the IC_{50} value by using a web-based tool [27].

[b] Not measured.

2.4 X-ray Crystallography

The rmGPb-ligand complexes of the most potent inhibitors from the kinetics studies (**10a-d**, **10h**) were determined using X-ray crystallography so as to decipher the interactions responsible for their potency. All compounds show similar potency for hlGPa and rmGPb and, the active sites in hlGP and rmGP are identical in terms of sequence and structure therefore conclusions based on structural data obtained with rmGPb are directly applicable to hlGPa.

The 2Fo-Fc and Fo-Fc electron density maps revealed that all five inhibitors were bound at the active site and clearly defined the position of each atom of the ligands (Figure 2). The superposition of the structures of free rmGPb and the rmGPb-inhibitor complexes over well-defined residues (18– 49, 262–312, 326–829) gave r.m.s.d. values of 0.15, 0.20, 0.17, 0.16, and 0.19 Å for the **10a**, **10b**, **10c**, **10d**, and **10h**, complexes, respectively, indicating that the binding of the inhibitors at the catalytic site did not trigger any major conformational change on the overall protein structure.

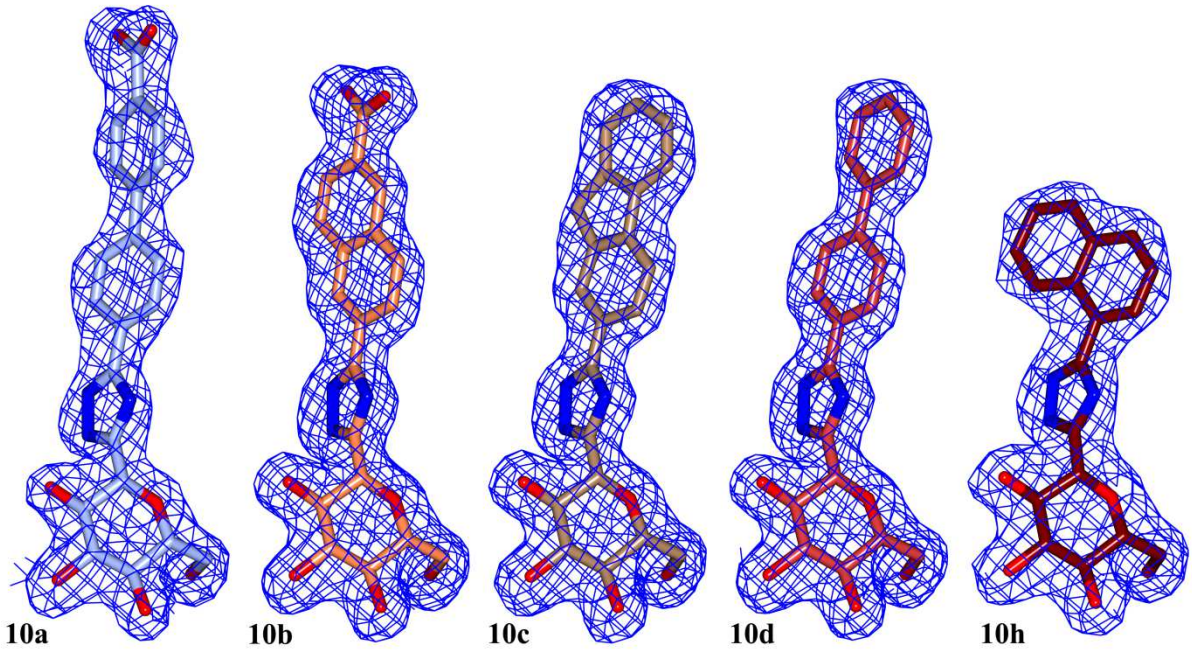

Figure 2. The REFMAC weighted 2Fo-Fc electron density maps of the bound ligands at the catalytic site contoured at 1.0 σ before the incorporation of the ligand molecules in the refinement process. The final models of the inhibitors are also shown.

Each of the inhibitors binds at the catalytic site by anchoring the glucose moiety at a location previously observed for α-D-glucose and other glucose-based inhibitors [20, 46-50]. There the glucose moiety engages in hydrogen bonding (Table 5) and van der Waals interactions almost identical to those that have been previously observed for similar glucose analogues. Furthermore, three conserved water molecules mediate hydrogen bond interactions between the glucopyranose moiety of each ligand and residues Asp283, Tyr573, Lys574, Thr671, Ala673, Thr676, and the phosphate group of the cofactor PLP.

Table 5: Potential hydrogen bond interactions of inhibitors with rmGPb residues at the catalytic site in the crystal. Hydrogen bonds are reported if the distance is less than 3.4 Å and the angle at the donor group is above 100°. Numbers shown are distances in Å.[a]

Inhibitor atom	Protein atoms	10a	10b	10c	10d	10h
O2'	Asn284 (ND2)	3.1	3.1	3.1	3.0	2.6
	Try573 (OH)	3.0	3.1	3.0	3.1	3.1
	Glu672 (OE2)	3.0	3.2	3.2	3.2	3.3
	Water (O)	2.9	3.0	2.9	3.0	2.8
	Water (O)	2.8	2.8	2.8	2.8	2.8
O3'	Glu672 (OE2)	2.6	2.6	2.6	2.7	2.7
	Ala673 (N)	3.3	3.2	3.2	3.2	3.3
	Ser674 (N)	3.1	3.1	3.1	3.1	3.1
	Gly675 (N)	3.1	3.2	3.2	3.2	3.3
O4'	Gly675 (N)	2.9	2.9	2.8	2.8	2.8
	Water (O)	2.6	2.6	2.6	2.6	2.6
O6'	His377 (ND1)	2.7	2.7	2.7	2.7	2.7
	Asn484 (ND2)	2.8	2.8	2.8	2.7	2.8
N2	His377 (O)	2.7	2.7	2.7	2.7	2.9
N5	Water (O)	3.0	3.0	2.9	2.9	2.8
O17	Glu287 (N)	3.2	-	-	-	-
	Gly288 (N)	3.1	-	-	-	-
	Water (O)	2.7	-	-	-	-

	Water (O)	3.3	-	-	-	-
	Water (O)	-	2.7	-	-	-
	Water (O)	-	3.0	-	-	-
O18	Asn282 (ND2)	3.1	3.3	-	-	-
	Water (O)	-	2.8	-	-	-
	Water (O)	2.8	-	-	-	-
Total		**21**	**19**	**15**	**15**	**15**

[a] Atom numbering is as displayed in Table 4.

The triazole linker participates in a hydrogen bond interaction with the main chain oxygen of His377 (Table 4), as was predicted by the modelling, and in water-mediated hydrogen bond interactions with the main chain nitrogen atoms of Gly135 and Leu136 through a conserved water molecule in all rmGPb ligand complexes. Similar interactions have been previously observed with other glucose derived inhibitors bound to rmGPb [46, 51], and the increased inhibitory potency of the 1,2,4-triazole compounds was ascribed to the hydrogen-bond forming capacity of the heterocyclic nitrogen atoms to the main chain oxygen of His377 and to water-mediated hydrogen bonding interactions with the sidechain atoms of Asp283 and the main chain atoms of Leu136.

In total, **10a**, **10b**, **10c**, **10d**, and **10h** engage in 116, 92, 90, 92, and 81 van der Waals interactions with protein residues at the active site of rmGPb, respectively (Figure 3). The phenyl ring A (*c.f.* Table 4) in **10a**, **10b**, **10c**, and **10d** is involved in van der Waals interactions with protein residues Glu88 and Asn284 while phenyl ring B (*c.f.* Table 4) is involved in van der Waals interactions with Asn282, Phe285, Phe286, and Arg292. These interactions have been also observed with other 1,2,4-triazole inhibitors and they were the source of the significant potency displayed by them [46, 51]. In addition the naphthyl ring of **10h** engages in van der Waals interactions with Glu88, Leu136, Asn283, and Ala383.

The carboxyl group of **10a** is involved in hydrogen bond interactions with the main chain atoms of Glu287 and Gly288 and the side chain of Asn282, while it also participates in water-mediated interactions with Lys289, Arg292, and Glu385 (Figure 3). The carboxyl group of **10b** participates in hydrogen bond interactions with the side chain of Asn282 and water-mediated interactions with Tyr280, Glu287, Gly288, Glu296, Arg292, and Glu385 (Figure 3).

All inhibitors except **10h** bind similar at the active site and do not seem to cause any significant conformational change. The binding of **10h** triggers a significant shift of the 280s loop (residues 282-289). The r.m.s. distance for all atoms of these residues between the rmGPb-**10c** and the rmGPb-**10h** complex structures is 1.0 Å with Asn282, Asn284, Phe285 and Glu287 being the residues with the greatest difference (Figure 4). This conformational change may arise from the different orientation of the naphthyl ring in **10h** with respect to the other four inhibitors studied here. The energy cost associated with this conformational change may also offer an explanation for the lower potency displayed by this compound in comparison to the potency of the other four inhibitors.

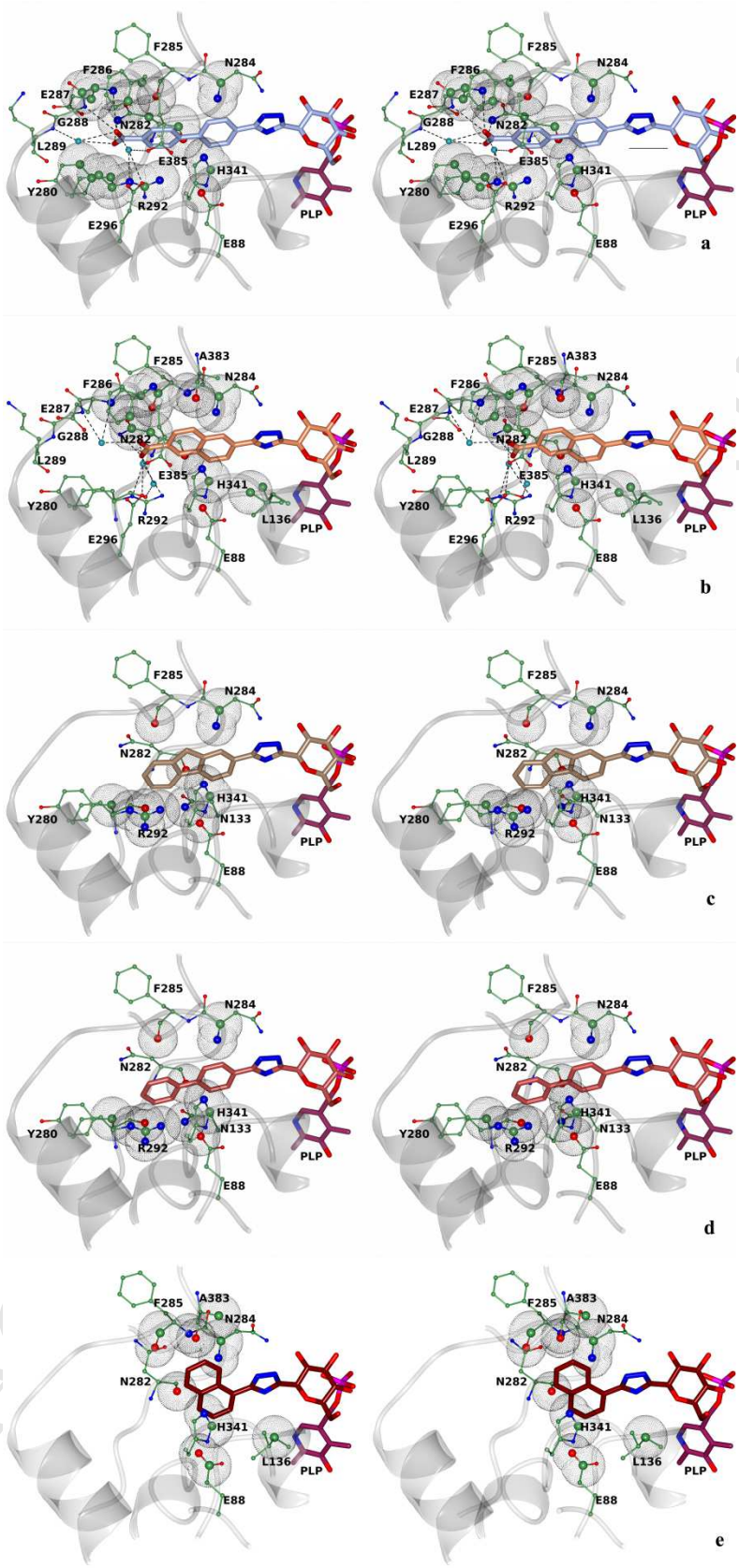

Figure 3. Diagrams of the binding of **10a** (a), **10b** (b), **10c** (c), **10d** (d), and **10h** (e) at the active site of rmGPb. Van der Waals interacting protein atoms are shown bigger and in meshed spheres.

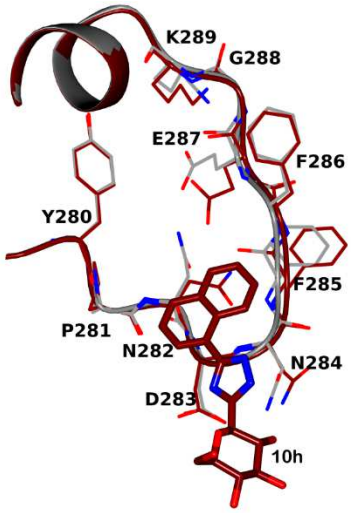

Figure 4. Superposition of the rmGPb-**10h** complex structure (maroon) and the free structure (grey).

The small differences in the inhibitory potency between inhibitors bearing a carboxyl group (**10a** and **10b**) and the unsubstituted non-polar ligands **10c** and **10d** could be attributed to the interactions of the carboxylates. Bulk desolvation effects will be associated with the negatively charged carboxylate going from the free unbound state to the bound state in the catalytic site. Additionally, the carboxyl groups upon binding hydrogen-bond a water molecule placing it in close proximity (~3.3 Å) to the phenyl ring of Tyr280 (**10a** complex) or Phe286 (~3.7 Å; **10b** complex), constituting unfavorable interactions. These unfavorable interactions are, however, counterbalanced by the hydrogen bond interactions of the carboxyl groups (O17 and O18, Table 5). In the **10c** and **10d** complexes no extra waters are brought into the catalytic site since they do not have any polar groups. Comparing **10c** and **10d**, their aromatic groups form 29 and 32 van der Waals interactions, respectively, at the rmGPb active site, indicating that they do not have significant differences in their protein interactions and hence they are almost equipotent. The better potency of inhibitor **10a** with respect to **10b** for rmGPb (and hlGPa) could be attributed to two additional hydrogen bond interactions of one of its carboxyl oxygen atoms with the main chain amides of Glu287 and Gly288 (Table 5).

2.5 Pharmacokinetics Predictions

Early monitoring of the pharmacokinetic profiles of lead compounds is recommended to help avoid potential for failure in later stage drug development trials. The absorption, distribution, metabolism and excretion (ADME) properties of our synthesized compounds were calculated using QikProp 3.5 [25], the results of which are shown in Table 6. An orally active drug should have no more than one violation of Lipinski's 'rule of five' [52] while for Jorgensen's 'rule of three' [53, 54] more drug-like molecules have fewer violations. All inhibitors except the least potent sulfamoyl derivative (**10f**) have just 0 or 1 violation of Lipinski's 'rule of five'. Considering Jorgensen's 'rule of three', there was a maximum of one violation for the ligands. While the Caco-2 cell permeability (> 22 nm s^{-1}) appears adequate for most ligands (~ 60 nm s^{-1}), it is flagged for **10a**, **10b** and the sulfamoyl derivative **10f**; the sensitive lipophilicity/solubility balance of β-D-glucose analogues with heterocyclic linkers has previously been highlighted [55, 56]. Polar surface areas (PSAs), however, are within the range of 95% of known drugs (**10f** excepted) although they are close to or above (**10a** and **10b**) Veber at al.'s [57] recommended value of < 140 $Å^2$ for oral bioavailability. With respect to the carboxylic acid moiety of **10a** and **10b**, a wide variety of endogenous substances such as amino acids and triglycerides possess this group and it is often part of the pharmacophore of diverse classes of therapeutic agents with more than 450 of carboxylic acid-containing drugs currently marketed worldwide [58]. A diminished ability to passively diffuse across biological membranes is more relevant in the context of central nervous system (CNS) drug discovery [58]. All other properties (Table 6) are satisfactory for the studied ligands. The predicted degree of binding to human serum albumin (log K_{hsa}) which affects bioavailability is -1.15 – -0.50 and within the range for 95% of known drugs (-1.5 – 1.5), while the log BB values (-3.6 – -2.1) predict that the inhibitors are unlikely to cross the blood-brain barrier.

3. Conclusions

Docking is widely used to distinguish active from inactives chemotypes in virtual screening studies. Here, GP inhibitor screening in the form of QM/MM docking (QM-PLD) has been applied to identify novel 3-(*β*-D-glucopyranosyl)-5-substituted-1,2,4-triazole derivatives. The advantage of a computationally driven (QM/MM docking) approach to candidate selection is highlighted, with eight out of the nine selected compounds selected for synthesis revealing either moderate or strong activity (K_i's < 100 µM) compared to only nine of eighteen in previous studies (Table 1). Five of the nine candidates had K_i's < 10 µM, our defined threshold for 'activity', with **10a-d** and **10h** potent low µM inhibitors (rmGPa, hlGPa) and **10a-c** on the high nM range for rmGPa. X-ray crystallography studies of the protein-ligand complexes revealed that the addition of polar groups such as carboxyl to the bulky aromatic ligand substituents in the β-cavity (although it offers additional hydrogen bond interactions with protein residues) does not lead to improved potency since this group also attracts water molecules that are placed in close proximity of hydrophobic residues. Structural studies indicate that improvement of the potency might otherwise arise by the replacement of the carboxyl groups with another non-polar chemical entity. Carbohydrate-based compounds and triazoles have proven to be important classes of compounds in the treatment or development of new clinical candidates for a number of conditions [59, 60]. The 3-(*β*-D-glucopyranosyl)-5-substituted-1,2,4-triazoles studied here are predicted to have drug-like potential with only permeability flagged as a potential issue to efficacy. However, the compounds have in general (for six of the nine synthesized) better predicted Caco-2 cell permeabilities (by a factor of 3) than previously reported glucose analogues [10, 55, 56] and accordingly are to be considered in further follow up experiments (cellular and *in vivo*) for efficacy.

Table 6. Results of ADME property predictions for the different tautomers of the 3-(β-D-glucopyranosyl)-5-substituted-1,2,4-triazole inhibitors studied in this work

Inhibitor	Lipinskis's Rule of Five and Violations (V)[b]					Jorgensen's Rule of Three and Violations (V)[b]				PSA [Å^2][c]	log K_{hsa}[d]	log *BB*[e]
	M_r [Da]	HBD[f]	HBA[g]	log $P_{(o/w)}$	V	Caco-2 [nm s^{-1}][h]	log *S*	NMP[i]	V			
	(<500)	(≤5)	(≤10)	(<5)		(>22)	(>-5.7)	(<7)		(<140 Å^2)		
10a	427.4	*6*	10	-0.2	1	*1.6**	-3.9	6	1	*185.1*	-0.85	-3.5*
10b	401.4	*6*	10	-0.7	1	*1.6**	-3.4	6	1	*185.0*	-0.94	-3.3*
10c	395.4	5	8	0.6	0	61.9	-4.2	*7*	1	135.6	-0.43	-2.2
10d	383.4	5	8	0.5	0	61.7	-3.9	6	0	135.6	-0.50	-2.2
10e	383.4	5	8	0.5	0	61.8	-3.9	6	0	135.6	-0.50	-2.2
10f	386.4	*7**	*11*	-2.8*	2	*2.9**	-2.6	6	1	*201.0**	-1.15	-3.6*
10h	357.4	5	8	-0.1	0	57.1	-3.4	6	0	137.0	-0.61	-2.1
10i	407.4	5	8	0.8	0	61.8	-4.3	*7*	1	135.6	-0.38	-2.2
10j	431.4	5	8	1.0	0	59.7	-4.5	*7*	1	137.0	-0.30	-2.2
Range[j]	**130-725**	**0-6**	**2-20**	**-2.0-6.5**	**-**	**<25 poor; > 500 great**	**-6.5-0.5**	**1-8**	**-**	**7-200**	**-1.5-1.5**	**-3.0-1.2**

[a] ADME data were calculated as described in the text using Qikprop 3.5; predicted properties outside the range for 95% of known drugs are indicated with an asterisk (*). [b] Rules as listed in the columns, with any violations of the rules highlighted in *italics*. [c] PSA represents the van der Waals (polar) surface areas of N and O atoms; recommended PSA < 140 Å^2 according to Veber et al. [57]. [d] log K_{hsa}: predicted binding to human serum albumin. [e] log *BB*: the predicted blood-brain barrier coefficient. [f] Number of hydrogen bond donors. [g] Number of hydrogen bond acceptors. [h] Caco-2 cell permeability. [i] Number of primary metabolites. [j] Range for 95% of known drugs [61].

4. Experimental

4.1 Computational details

4.1.1 Protein Preparation

The initial setup of the GPb receptor for docking was performed using Schrodinger's "Protein Preparation Wizard" [25] and the solved co-crystallized complex with *N*-(2-naphthyl)-*N´*-(*β*-D-glucopyranosyl)urea [5]. Water molecules within 5 Å of the native ligand were initially retained but deleted for subsequent docking. Bond orders were assigned and hydrogen atoms added, with protonation states for basic and acidic residues based on residue pK_a values at normal pH (7.0) calculated using PROPKA [62]. Subsequent optimization of hydroxyl groups, histidine protonation states and C/N atom "flips", and side-chain O/N atom flips of Asn and Gln was based on optimizing hydrogen bonding patterns. The phosphate in pyridoxal-phosphate (PLP) was assigned in monoanionic form. Finally, an "Impref" minimization of the GPb complex was performed using the OPLS-AA(2005) force field [63] to remove steric clashes and bad contacts but with heavy atoms constrained to within 0.3 Å (RMSD) of their crystallographic positions.

4.1.2 Ligand Preparation

Training and screening set ligands were prepared using a combination of Maestro, LigPrep 3.5 and CombiGlide 3.8 [25]. For creation of the screening set database ligands consisting of diverse –R groups, "purchasable" acids (R-COOH), acid chlorides (R-COCl) and aldehydes (R-CHO) were downloaded from the ZINC docking database [26]. The following criteria were used as filters so that the final proposed ligands contained aryl substituents and were 'drug-like':[52, 57] MWs ≤ 200, 224, and 240 Da with benzoyl chloride, benzoic acid and benzaldehyde used as substructures, respectively; 0 ≤ rotatable bonds ≤ 4. Using CombiGlide, the resulting reagents were 'reacted' with the 3-(*β*-D-glucopyranosyl)-1,2,4-triazole 'core' to

yield the final 3-(*β*-D-glucopyranosyl)-5-substituted-1,2,4-triazoles. 2335 distinct ligands constituted the screening set. LigPrep 3.5 generation of tautomers and favorable ionization states at pH = 7 ± 2 of the ligands resulted in three distinct tautomers of the triazole moiety (H on each of three N atoms); however, with only one triazole tautomer favored for the binding of all training set ligands to GPb (H on N2), only this tautomeric state was considered for docking of the screening set ligands.

4.1.3 Docking Calculations

Training Set Ligands: Flexible-ligand docking calculations were performed using Glide 6.8 in both standard- (SP) and extra-precision (XP) modes, as well as with QM-PLD [25, 64]. In the docking calculations with Glide, the shape and properties of the GPb catalytic site were first mapped onto grids with dimensions of 26.7 × 26.7 × 26.7 Å centred on the native co-crystallized ligand. Positional constraints on the four glucose -OH oxygen atoms were applied (radius 1.5 Å) [65]. Standard parameters were otherwise applied for the Glide-SP and XP docking calculations. Post-docking minimization of the ligand poses was performed (with strain correction) and a maximum of 3 poses per ligand saved. Poses were ranked by 'docking score'. For the QM-PLD calculations, atomic partial charges of the output docking poses from Glide XP docking were reparametrized in the 'field' of the receptor (ESP fit charges) using QSite 6.8 [25] and single point energy QM/MM calculations. The ligands were then redocked using Glide-XP.

Virtual Screening: Docking of the screening set ligands was performed using QM-PLD and with the same settings as for the training set ligands described above.

4.1.4 ADME Property Predictions

QikProp from Schrödinger [25] was used for the ADME property predictions. Specifically, Lipinski's rules of five [52] (MW < 500, log P < 5, HBA ≤ 10, and HBD ≤ 5) and Jorgensen's

rule of three [53, 54] (log S > -5.7, Caco-2 permeability > 22 nm/s, number of primary metabolites < 7) were applied to predict oral bioavailability. Calculations were performed in normal mode and are reported for the 1,2,4-triazole binding most stable tautomer (Table 1), with test calculations here and from previous studies [56] on *β*-D-glucopyranosyl 1,2,4-triazole derivatives showing that the tautomeric state of the triazole has limited effect on the property predictions.

4.2 Synthesis

4.2.1 General methods

Anhydrous toluene, *m*-xylene, $CHCl_3$, EtOAc, CH_3CN (P_2O_5), THF (Na, benzophenone), pyridine (KOH), MeOH (Mg) were prepared by distillation from the indicated drying agent. Reagents were purchased from commercial suppliers (Sigma-Aldrich, TCI, Alfa Aesar) and used without further purification. TLC was carried out on precoated plates (DC-Alurolle Kieselgel 60, F_{254}, Merck), and the spots were visualized under UV light and by gentle heating. Column chromatography was performed on silica gel (Kieselgel 60, 63-200 µm, Molar Chemicals). ^1H, ^{13}C NMR spectra were recorded on Bruker DRX 360 and Bruker DRX 400 spectrometers. TMS (^1H) or resonance peak of the solvent (^{13}C) was used as reference. Mass spectra were obtained by a Bruker micrOTOF-Q instrument. Microanalyses were performed on an Elementar Vario Micro Cube. Optical rotations were determined with a Perkin-Elmer 241 polarimeter at rt.

4.2.2 General procedure I for the synthesis of 4-benzyl-3-(2,3,4,6-tetra-*O*-benzoyl-β-D-glucopyranosyl)-5-substituted-1,2,4-triazoles (6)

The solution of an *N*-benzyl-arenecarboxamide (**5**, 2 equiv.) in $SOCl_2$ (5 mL/mmol) was heated at boiling temp. for 2 h then the excess of $SOCl_2$ was removed under diminished

pressure. The residue was dissolved in anhydrous toluene and evaporated in order to remove the traces of the reagent. 5-(2,3,4,6-Tetra-*O*-benzoyl-β-D-glucopyranosyl)tetrazole (**1**, 1 equiv.) in anhydrous *m*-xylene (15 mL/mmol) was added and the mixture was refluxed until disappearance of the tetrazole (TLC, 4:1 toluene-AcOH). After evaporation of the solvent the residue was purified by column chromatography.

4.2.3 General procedure II for the synthesis of 3-(2,3,4,6-tetra-*O*-benzoyl-β-D-glucopyranosyl)-5-substituted-1,2,4-triazoles (7) from *N*^{1}-tosyl-*C*-(2,3,4,6-tetra-*O*-benzoyl-β-D-glucopyranosyl)formamidrazone (2)

N^1-Tosyl-*C*-(2,3,4,6-tetra-*O*-benzoyl-β-D-glucopyranosyl)formamidrazone (**2**) was dissolved in anhydrous $CHCl_3$ (15 mL/mmol) and anhydrous pyridine (3.0 equiv.) was added. The mixture was cooled in an ice bath, and the solution of an aroyl chloride (3.0 equiv.) in anhydrous $CHCl_3$ (5 mL/mmol) was added dropwise over 15 minutes. Subsequently, the mixture was stirred at rt and monitored by TLC (3:1 EtOAc-hexane). After total consumption of the starting material (2 days) the mixture was diluted with $CHCl_3$ and extracted with water. The organic phase was dried over $MgSO_4$ and concentrated under diminished pressure. The obtained residue was dissolved in THF (20 mL/mmol) and TBAF (1 M solution in THF, 2.0 equiv.) was added. The reaction mixture was boiled for 24 h and then it was concentrated and purified by column chromatography.

4.2.4 General procedure III for the preparation of *N*-(2,3,4,6-tetra-*O*-benzoyl-β-D-glucopyranosylcarbonyl)thioamides (8)

A mixture of *C*-(2,3,4,6-tetra-*O*-benzoyl-β-D-glucopyranosyl)formic acid (**3**) and $SOCl_2$ (10 mL/mmol) was boiled under reflux for two hours, then the excess of the reagent was removed under diminished pressure. Last traces of $SOCl_2$ were removed by co-evaporations with dry

toluene. The resulting acid chloride (**4**) was dissolved in anhydrous CH_3CN (15 mL/mmol), and a solution or a suspension of the corresponding thioamide (1.2 equiv.) and pyridine (1.2 equiv.) in anhydrous CH_3CN (30-120 mL/mmol depending on the solubility of the thioamide) was added dropwise over 20 minutes. The reaction mixture was stirred at rt, and monitored by TLC (1:1 hexane-EtOAc). After complete conversion the solvent was removed and the residue was purified by column chromatography.

4.2.5 General procedure IV for the preparation of 3-(2,3,4,6-tetra-*O*-benzoyl-β-D-glucopyranosyl)-5-substituted-1,2,4-triazoles (7) from *N*-(2,3,4,6-tetra-*O*-benzoyl-β-D-glucopyranosylcarbonyl)thioamides (8)

To a solution of an *N*-(2,3,4,6-tetra-*O*-benzoyl-β-D-glucopyranosylcarbonyl)thioamide (**8**) in anhydrous pyridine (10 mL/mmol) hydrazine monohydrate (1.2 equiv.) was added, and the reaction mixture was stirred at rt. After disappearance of the starting material (monitored by TLC, 1:1 hexane-EtOAc) the solvent was removed and the residue was purified by column chromatography.

N-Benzyl and *O*-benzoyl protecting groups were removed by standard methods to give the test compounds **10**. Detailed procedures for deprotections as well as compound characterization are described in the Supporting Information.

4.3 Kinetics

Rabbit muscle GPb (rmGPb) was purified from rabbit skeletal muscle following the protocol developed by Fischer & Krebs [66] with slight modifications [67] while rmGPa was produced by phosphorylation of rmGPb [51]. Human liver GPa (hlGPa) was produced following a previously described protocol [51]. Kinetic studies were performed at 30 °C in the direction of glycogen synthesis using 3 μg/mL of the rabbit muscle enzymes, or 1 μg/mL hlGPa in a 30

mM imidazole/HCl buffer (pH 6.8) containing 60 mM KCl, 0.6 mM EDTA, and 0.6 mM dithiothreitol, using constant concentrations of glycogen (0.2% w/v), AMP (1 mM; only for the rmGPb experiments), and various concentrations of Glc-1-P and inhibitors. Initial velocities were calculated from the pseudo-first order rate constants measuring the release of orthophosphate ions spectrophotometrically [68] at five time-intervals. For the calculation and statistical evaluation of the kinetic parameters, the non-linear regression program Grafit [69] was employed.

4.4 X-ray Crystallography

rmGPb-inhibitor complexes were formed by diffusion of 10 mM solution of the inhibitors in the crystallization media supplemented with DMSO (15 %, v/v) in preformed rmGPb crystals [70] at room temperature for 3 hours prior to data collection. X-ray diffraction data were collected using synchrotron radiation on station I04 (λ=0.9795 Å) at Diamond Synchrotron Radiation Source in Oxford, U.K. at room temperature on a Pilatus 6M detector. To avoid crystal radiation damage the crystal was translated five times. Crystal orientation, integration of reflections, inter-frame scaling, partial reflection summation, and data reduction was performed by the program XDS [71]. Scaling and merging of intensities were performed by Aimless [72] and the optimum resolution was selected based on the $CC^{1/2}$ criterion [73]. Crystallographic refinement of the complexes was performed by maximum-likelihood methods using REFMAC [74] with starting model the structure of the native T state rmGPb complex determined at 1.9 Å resolution (Leonidas et al, unpublished results). Ligand molecule coordinates and topologies were constructed using JLigand [75] and they were fitted to the electron density maps by adjusting of their torsion angles. A summary of the data processing and refinement statistics for the inhibitor complex structures is given in Table 1. The refinement was validated by the PDB_REDO server [76]. As there were more than 5 reflections per atom available, both an isotropic and an anisotropic B-factor model were

considered, and the isotropic B-factor model was selected based on the Hamilton R ratio test. The stereochemistry of the protein residues was validated by MolProbity [77]. Hydrogen bonds and van der Waals interactions were calculated with the program CONTACT as implemented in CCP4 [78] applying a distance cut off 4.1 Å and 4.0 Å, respectively. Figures were prepared with CCP4 Molecular Graphics [79]. The coordinates of the new structures have been deposited with the RCSB Protein Data Bank (http://www.rcsb.org/pdb) with codes as presented in Table 7.

Acknowledgments

We would like to thank Dr A.L. Kantsadi for help during X-ray diffraction data collection. This work was supported in part by the Postgraduate Programmes ‘‘Biotechnology-Quality assessment in Nutrition and the Environment”, ‘‘Application of Molecular Biology-Molecular Genetics-Molecular Markers”, Department of Biochemistry and Biotechnology, University of Thessaly. Work at the Synchrotron Radiation Source, Diamond, Oxford, U.K., was supported from the EU H2020 Programme iNext (Project ID: 653706). E.K. and G.A.S. would like to acknowledge financial support from the Hellenic State Scholarships Foundation and the action “Support of human research resources through doctoral research” funded by the "Operational Programme Education and Lifelong Learning" co-funded by the European Social Fund (ESF) and National Resources. Synthetic work was financed by the grants OTKA PD105808, PD 121406, and the project GINOP-2.3.2-15-2016-00008 supported by the EU and co-financed by the European Regional Development Fund.

Supplementary Information:

Supplementary information related to this article is included.

Table 7: Summary of the diffraction data processing and refinement statistics for the rmGPb inhibitor complexes. Values in parentheses are for the outermost shell.

rmGPb complex	**10a**	**10b**	**10c**	**10d**	**10h**
Data Processing and collection statistics					
Resolution (Å)	128 – 2.20 (2.27 – 2.20)	129 – 1.90 (1.94 – 1.90)	129 – 1.90 (1.94 – 1.90)	116 – 1.90 (1.94 – 1.90)	91 – 2.20 (2.27 – 2.20)
Reflections measured	528815	1141897	1149248	1146204	729941
Unique reflections	49885	76655	75805	77397	50194
R_{merge}	0.229 (0.742)	0.163 (0.799)	0.162 (0.703)	0.143 (0.996)	0.213 (1.137)
Completeness (%)	99.8 (99.7)	99.5 (98.9)	98.1 (96.9)	100 (100)	100 (100)
$< I/\sigma(I) >$	10.3 (5.5)	10.8 (3.4)	11.6 (4.1)	12.2 (3.1)	9.1 (2.8)
Multiplicity	10.6 (9.7)	14.9 (15.3)	15.2 (15.7)	14.8 (15.1)	14.5 (14.9)
$CC^{1/2}$	0.984 (0.946)	0.993 (0.939)	0.995 (0.960)	0.995 (0.933)	0.954 (0.885)
B Wilson ($Å^2$)	23.1	28.7	27.4	29.9	30.3
Reflections used for refinement	47423	72835	72024	73452	47694
No of water molecules	276	250	248	242	203
No of ligand atoms	31	29	29	28	26
R (R_{free}) (%)	13.6 (16.7)	13.7 (16.1)	13.3 (16.0)	13.5 (15.6)	14.2 (17.2)
Outer shell R (R_{free}) (%)	15.7 (19.4)	18.1 (21.9)	16.9 (21.9)	19.0 (22.3)	20.7 (24.4)

r.m.s.d. in bond lengths (Å)	0.009	0.010	0.017	0.010	0.010
r.m.s.d. in bond angles (°)	1.27	1.31	1.71	1.32	1.35
Average B (Å^2)					
Protein atoms	21.8	28.8	27.4	30.0	30.5
Water molecules	34.6	43.1	40.6	42.8	41.1
Ligand atoms	26.7	26.9	28.2	30.1	33.0
PDB entry	6F3J	6F3L	6F3R	6F3S	6F3U

References

[1] World Health Organisation. www.who.int (accessed 12/12/2017).

[2] M. Brownlee, Biochemistry and molecular cell biology of diabetic complications, Nature, 414 (2001) 813-820.

[3] N.G. Oikonomakos, Glycogen phosphorylase as a molecular target for type 2 diabetes therapy, Current Protein & Peptide Science, 3 (2002) 561-586.

[4] J.M. Hayes, A.L. Kantsadi, D.D. Leonidas, Natural products and their derivatives as inhibitors of glycogen phosphorylase: potential treatment for type 2 diabetes, Phytochem. Rev., 13 (2014) 471-498.

[5] L. Somsák, K. Czifrák, M. Tóth, É. Bokor, E.D. Chrysina, K.M. Alexacou, J.M. Hayes, C. Tiraidis, E. Lazoura, D.D. Leonidas, S.E. Zographos, N.G. Oikonomakos, New inhibitors of glycogen phosphorylase as potential antidiabetic agents, Curr Med Chem, 15 (2008) 2933-2983.

[6] J.M. Hayes, Computer-aided discovery of glycogen phosphorylase inhibitors exploiting natural products, in: G. Brahmachari (Ed.) Discovery and development of antidiabetic agents from natural products, Elsevier, 2017, pp. 29-62.

[7] E.D. Chrysina, M.N. Kosmopolou, C. Tiraidis, R. Kardarakis, N. Bischler, D.D. Leonidas, Z. Hadady, L. Somsák, T. Docsa, P. Gergely, N.G. Oikonomakos, Kinetic and crystallographic studies on 2-(β-D-glucopyranosyl)-5-methyl-1,3,4-oxadiazole, -benzothiazole, and -benzimidazole, inhibitors of muscle glycogen phosphorylase *b*. Evidence for a new binding site, Protein Science, 14 (2005) 873-888.

[8] A.L. Kantsadi, A. Apostolou, S. Theofanous, G.A. Stravodimos, E. Kyriakis, V.A. Gorgogietas, D.S.M. Chatzileontiadou, K. Pegiou, V.T. Skamnaki, D. Stagos, D. Kouretas, A.-M.G. Psarra, S.A. Haroutounian, D.D. Leonidas, Biochemical and biological assessment of the inhibitory potency of extracts from vinification byproducts of Vitis vinifera extracts against glycogen phosphorylase, Food Chem. Toxicol., 67 (2014) 35-43.

[9] G.A. Stravodimos, B.A. Chetter, E. Kyriakis, A.L. Kantsadi, D.S. Chatzileontiadou, V.T. Skamnaki, A. Kato, J.M. Hayes, D.D. Leonidas, Phytogenic Polyphenols as Glycogen Phosphorylase Inhibitors: The Potential of Triterpenes and Flavonoids for Glycaemic Control in Type 2 Diabetes, Curr Med Chem, 24 (2017) 384-403.

[10] A.L. Kantsadi, J.M. Hayes, S. Manta, V.T. Skamnaki, C. Kiritsis, A.-M.G. Psarra, Z. Koutsogiannis, A. Dimopoulou, S. Theofanous, N. Nikoleousakos, P. Zoumpoulakis, M. Kontou, G. Papadopoulos, S.E. Zographos, D. Komiotis, D.D. Leonidas, The s-Hole Phenomenon of Halogen Atoms Forms the Structural Basis of the Strong Inhibitory Potency of C5 Halogen Substituted Glucopyranosyl Nucleosides towards Glycogen Phosphorylase b, ChemMedChem, 7 (2012) 722-732.

[11] V. Parmenopoulou, A.L. Kantsadi, V.G. Tsirkone, D.S.M. Chatzileontiadou, S. Manta, S.E. Zographos, C. Molfeta, G. Archontis, L. Agius, J.M. Hayes, D.D. Leonidas, D. Komiotis, Structure based inhibitor design targeting glycogen phosphorylase b. Virtual screening, synthesis, biochemical and biological assessment of novel N-acyl-beta-D-glucopyranosylamines, Bioorganic & Medicinal Chemistry, 22 (2014) 4810-4825.

[12] T. Docsa, K. Czifrak, C. Huse, L. Somsak, P. Gergely, Effect of glucopyranosylidene-spiro-thiohydantoin on glycogen metabolism in liver tissues of streptozotocin-induced and obese diabetic rats, Mol Med Rep, 4 (2011) 477-481.

[13] L. Nagy, T. Docsa, A. Brunyánszki, M. Szántó, C. Hegedős, J. Marton, B. Kónya, L. Virág, L. Somsák, P. Gergely, P. Bai, Glycogen phosphorylase inhibitor *N*-(3,5-dimethyl-benzoyl)-*N*'-(β-D-glucopyranosyl) urea improves glucose tolerance under normoglycemic and diabetic conditions through rearranging hepatic metabolism, PLoS ONE, 8 (2013) e69420.

[14] W.H. Martin, D.J. Hoover, S.J. Armento, I.A. Stock, R.K. McPherson, D.E. Danley, R.W. Stevenson, E.J. Barrett, J.L. Treadway, Discovery of a human liver glycogen phosphorylase inhibitor that lowers blood glucose in vivo, Proceedings of the National Academy of Sciences of the United States of America, 95 (1998) 1776-1781.

[15] D. Goyard, B. Konya, A.S. Chajistamatiou, E.D. Chrysina, J. Leroy, S. Balzarin, M. Tournier, D. Tousch, P. Petit, C. Duret, P. Maurel, L. Somsak, T. Docsa, P. Gergely, J.P. Praly, J. Azay-Milhau, S. Vidal, Glucose-derived spiro-isoxazolines are anti-hyperglycemic agents against type 2 diabetes through glycogen phosphorylase inhibition, Eur J Med Chem, 108 (2016) 444-454.

[16] T. Docsa, B. Marics, J. Nemeth, C. Huse, L. Somsak, P. Gergely, B. Peitl, Insulin Sensitivity is Modified by a Glycogen Phosphorylase Inhibitor: Glucopyranosylidene-Spiro-Thiohydantoin in Streptozotocin-Induced Diabetic Rats, Curr Top Med Chem, 15 (2015) 2390-2394.

[17] L. Xu, H. Sun, Pharmacological Manipulation of Brain Glycogenolysis as a Therapeutic Approach to Cerebral Ischemia, Mini-Rev Med Chem, 10 (2010) 1188-1193.

[18] C.E. Zois, E. Favaro, A.L. Harris, Glycogen metabolism in cancer, Biochemical Pharmacology, 92 (2014) 3-11.

[19] T. Guan, Y.S. Qian, X.Z. Tang, M.H. Huang, L.F. Huang, Y.M. Li, H.B. Sun, Maslinic Acid, a Natural Inhibitor of Glycogen Phosphorylase, Reduces Cerebral Ischemic Injury in Hyperglycemic Rats by GLT-1 Up-Regulation, J Neurosci Res, 89 (2011) 1829-1839.

[20] L. Somsák, Glucose derived inhibitors of glycogen phosphorylase, Comptes Rendus Chimie, 14 (2011) 211-223.

[21] J.P. Praly, S. Vidal, Inhibition of Glycogen Phosphorylase in the Context of Type 2 Diabetes, with Focus on Recent Inhibitors Bound at the Active Site, Mini-Rev Med Chem, 10 (2010) 1102-1126.

[22] E. Bokor, E. Kyriakis, T.G.A. Solovou, C. Koppany, A.L. Kantsadi, K.E. Szabo, A. Szakacs, G.A. Stravodimos, T. Docsa, V.T. Skamnaki, S.E. Zographos, P. Gergely, D.D. Leonidas, L. Somsak, Nanomolar Inhibitors of Glycogen Phosphorylase Based on beta-d-Glucosaminyl Heterocycles: A Combined Synthetic, Enzyme Kinetic, and Protein Crystallography Study, J Med Chem, 60 (2017) 9251-9262.

[23] S. Kun, É. Bokor, G. Varga, B. Szőcs, A. Páhi, K. Czifrák, M. Tóth, L. Juhász, T. Docsa, P. Gergely, L. Somsák, New synthesis of 3-(β-D-glucopyranosyl)-5-substituted-1,2,4-triazoles, nanomolar inhibitors of glycogen phosphorylase, Eur J Med Chem, 76 (2014) 567-579.

[24] É. Bokor, T. Docsa, P. Gergely, L. Somsák, *C*-Glucopyranosyl-1,2,4-triazoles as new potent inhibitors of glycogen phosphorylase, Acs Med Chem Lett, 4 (2013) 612-615.

[25] Schrödinger, in, LLC, New York, NY, 2014.

[26] J.J. Irwin, T. Sterling, M.M. Mysinger, E.S. Bolstad, R.G. Coleman, ZINC: A Free Tool to Discover Chemistry for Biology, Journal of Chemical Information and Modeling, 52 (2012) 1757-1768.

[27] R.Z. Cer, U. Mudunuri, R. Stephens, F.J. Lebeda, IC50-to-K-i: a web-based tool for converting IC50 to K-i values for inhibitors of enzyme activity and ligand binding, Nucleic Acids Research, 37 (2009) W441-W445.

[28] W.J. Xu, A.J. Lucke, D.P. Fairlie, Comparing sixteen scoring functions for predicting biological activities of ligands for protein targets, J Mol Graph Model, 57 (2015) 76-88.

[29] K.L. Damm-Ganamet, R.D. Smith, J.B. Dunbar, J.A. Stuckey, H.A. Carlson, CSAR Benchmark Exercise 2011-2012: Evaluation of Results from Docking and Relative Ranking of Blinded Congeneric Series, Journal of Chemical Information and Modeling, 53 (2013) 1853-1870.

[30] D.A. Pearlman, P.S. Charifson, Are free energy calculations useful in practice? A comparison with rapid scoring functions for the p38 MAP kinase protein system, Journal of Medicinal Chemistry, 44 (2001) 3417-3423.

[31] R.C. Team, R: A language and environment for statistical computing in: R Foundation for Statistical Computing, Vienna, Austria, 2017.

[32] J. Du, H.J. Sun, L.L. Xi, J.Z. Li, Y. Yang, H.X. Liu, X.J. Yao, Molecular Modeling Study of Checkpoint Kinase 1 Inhibitors by Multiple Docking Strategies and Prime/MM-GBSA Calculation, Journal of Computational Chemistry, 32 (2011) 2800-2809.

[33] A.E. Cho, J.Y. Chung, M. Kim, K. Park, Quantum mechanical scoring for protein docking, Journal of Chemical Physics, 131 (2009).

[34] M. Benltifa, J.M. Hayes, S. Vidal, D. Gueyrard, P.G. Goekjian, J.P. Praly, G. Kizilis, C. Tiraidis, K.M. Alexacou, E.D. Chrysina, S.E. Zographos, D.D. Leonidas, G. Archontis, N.G. Oikonomakos, Glucose-based spiro-isoxazolines: A new family of potent glycogen phosphorylase inhibitors, Bioorganic & Medicinal Chemistry, 17 (2009) 7368-7380.

[35] J.Y. Chung, J.M. Hah, A.E. Cho, Correlation between Performance of QM/MM Docking and Simple Classification of Binding Sites, Journal of Chemical Information and Modeling, 49 (2009) 2382-2387.

[36] M.M. Francl, W.J. Pietro, W.J. Hehre, J.S. Binkley, M.S. Gordon, D.J. Defrees, J.A. Pople, Self-Consistent Molecular-Orbital Methods .23. A Polarization-Type Basis Set for 2nd-Row Elements, Journal of Chemical Physics, 77 (1982) 3654-3665.

[37] W.J. Hehre, Ditchfie.R, J.A. Pople, Self-Consistent Molecular-Orbital Methods .12. Further Extensions of Gaussian-Type Basis Sets for Use in Molecular-Orbital Studies of Organic-Molecules, Journal of Chemical Physics, 56 (1972) 2257-&.

[38] A.D. Becke, Density-Functional Thermochemistry .3. The Role of Exact Exchange, Journal of Chemical Physics, 98 (1993) 5648-5652.

[39] C.T. Lee, W.T. Yang, R.G. Parr, Development of the Colle-Salvetti Correlation-Energy Formula into a Functional of the Electron-Density, Physical Review B, 37 (1988) 785-789.

[40] P.J. Stephens, F.J. Devlin, C.F. Chabalowski, M.J. Frisch, Ab-Initio Calculation of Vibrational Absorption and Circular-Dichroism Spectra Using Density-Functional Force-Fields, Journal of Physical Chemistry, 98 (1994) 11623-11627.

[41] B. Szocs, E. Bokor, K.E. Szabo, A. Kiss-Szikszai, M. Toth, L. Somsak, Synthesis of 5-aryl-3-C-glycosyl- and unsymmetrical 3,5-diaryl-1,2,4-triazoles from alkylidene-amidrazones, Rsc Adv, 5 (2015) 43620-43629.

[42] K.E. Szabo, A. Pahi, L. Somsak, C-Glycosyl 1,2,4-triazoles: Synthesis of the 3-beta-D-glucopyranosyl-1,5-disubstituted and 5-beta-D-glucopyranosyl-1,3-disubstituted variants, Tetrahedron, 73 (2017) 3810-3822.

[43] E. Bokor, A. Fekete, G. Varga, B. Szocs, K. Czifrak, I. Komaromi, L. Somsak, C-(beta-D-Glucopyranosyl)formamidrazones, formic acid hydrazides and their transformations into 3-(beta-D-glucopyranosyl)-5-substituted-1,2,4-triazoles: a synthetic and computational study, Tetrahedron, 69 (2013) 10391-10404.

[44] S. Kun, G.Z. Nagy, M. Toth, L. Czecze, N.V.N. Albert, T. Docsa, P. Gergely, M.D. Charavgi, P.V. Skourti, E.D. Chrysina, T. Patonay, L. Somsak, Synthesis of variously coupled conjugates of D-glucose, 1,3,4-oxadiazole, and 1,2,3-triazole for inhibition of glycogen phosphorylase, Carbohyd Res, 346 (2011) 1427-1438.

[45] K. Czifrak, P. Szilagyi, L. Somsak, Anomeric alpha-azido acid (2-azido-2-deoxy-hept-2-ulopyranosonic acid) derivatives en route to peptides incorporating sugar amino acids, Tetrahedron-Asymmetr, 16 (2005) 127-141.

[46] A.L. Kantsadi, G.A. Stravodimos, E. Kyriakis, D.S.M. Chatzileontiadou, T.G.A. Solovou, S. Kun, E. Bokor, L. Somsak, D.D. Leonidas, van der Waals interactions govern C-beta-d-glucopyranosyl triazoles' nM inhibitory potency in human liver glycogen phosphorylase, J Struct Biol, 199 (2017) 57-67.

[47] A.L. Kantsadi, S. Manta, A.M. Psarra, A. Dimopoulou, C. Kiritsis, V. Parmenopoulou, V.T. Skamnaki, P. Zoumpoulakis, S.E. Zographos, D.D. Leonidas, D. Komiotis, The binding of C5-alkynyl and alkylfurano[2,3-d]pyrimidine glucopyranonucleosides to glycogen phosphorylase b: synthesis, biochemical and biological assessment, Eur J Med Chem, 54 (2012) 740-749.

[48] A.L. Kantsadi, E. Bokor, S. Kun, G.A. Stravodimos, D.S. Chatzileontiadou, D.D. Leonidas, E. Juhasz-Toth, A. Szakacs, G. Batta, T. Docsa, P. Gergely, L. Somsak, Synthetic, enzyme kinetic, and protein crystallographic studies of C-beta-d-glucopyranosyl pyrroles and

imidazoles reveal and explain low nanomolar inhibition of human liver glycogen phosphorylase, Eur J Med Chem, 123 (2016) 737-745.

[49] J.L. Martin, L.N. Johnson, S.G. Withers, Comparison of the binding of glucose and glucose 1-phosphate derivatives to T-state glycogen phosphorylase b, Biochemistry, 29 (1990) 10745-10757.

[50] J.L. Martin, K. Veluraja, K. Ross, L.N. Johnson, G.W.J. Fleet, N.G. Ramsden, I. Bruce, M.G. Orchard, N.G. Oikonomakos, A.C. Papageorgiou, D.D. Leonidas, H.S. Tsitoura, Glucose analogue inhibitors of glycogen phosphorylase: The design of potential drugs for diabetes, Biochemistry (USA), 30 (1991) 10101-10116.

[51] E. Kyriakis, T.G.A. Solovou, S. Kun, K. Czifrák, B. Szőcs, L. Juhász, E. Bokor, G.A. Stravodimos, A.L. Kantsadi, D.S.M. Chatzileontiadou, V.T. Skamnaki, L. Somsák, D.D. Leonidas, Probing the β-pocket of the active site of human liver glycogen phosphorylase with 3-(C-β-D-glucopyranosyl)-5-(4-substituted-phenyl)-1,2,4-triazole inhibitors Bioorg. Chem., (2017).

[52] C.A. Lipinski, F. Lombardo, B.W. Dominy, P.J. Feeney, Experimental and computational approaches to estimate solubility and permeability in drug discovery and development settings, Advanced Drug Delivery Reviews, 23 (1997) 3-25.

[53] W.L. Jorgensen, E.M. Duffy, Prediction of drug solubility from Monte Carlo simulations, Bioorganic and Medicinal Chemistry Letters, 10 (2000) 1155-1158.

[54] W.L. Jorgensen, E.M. Duffy, Prediction of drug solubility from structure, Advanced Drug Delivery Reviews, 54 (2002) 355-366.

[55] M. Polyák, G. Varga, B. Szilágyi, L. Juhász, T. Docsa, P. Gergely, J. Begum, J.M. Hayes, L. Somsák, Synthesis, enzyme kinetics and computational evaluation of N-(beta-D-glucopyranosyl) oxadiazolecarboxamides as glycogen phosphorylase inhibitors, Bioorganic and Medicinal Chemistry, 21 (2013) 5738-5747.

[56] J. Begum, G. Varga, T. Docsa, P. Gergely, J.M. Hayes, L. Juhasz, L. Somsak, Computationally motivated synthesis and enzyme kinetic evaluation of N-(beta-D-

glucopyranosyl)-1,2,4-triazolecarboxamides as glycogen phosphorylase inhibitors, Medchemcomm, 6 (2015) 80-89.

[57] D.F. Veber, S.R. Johnson, H.Y. Cheng, B.R. Smith, K.W. Ward, K.D. Kopple, Molecular properties that influence the oral bioavailability of drug candidates, Journal of Medicinal Chemistry, 45 (2002) 2615-2623.

[58] C. Ballatore, D.M. Huryn, A.B. Smith, Carboxylic Acid (Bio)Isosteres in Drug Design, Chemmedchem, 8 (2013) 385-395.

[59] C.H. Zhou, Y. Wang, Recent Researches in Triazole Compounds as Medicinal Drugs, Curr Med Chem, 19 (2012) 239-280.

[60] V.K. Tiwari, R.C. Mishra, A. Sharma, R.P. Tripathi, Carbohydrate based Potential Chemotherapeutic Agents: Recent Developments and their Scope in Future Drug Discovery, Mini-Rev Med Chem, 12 (2012) 1497-1519.

[61] QikProp, in, Schrödinger, LLC, New York, NY, 2012.

[62] C.R. Sondergaard, M.H.M. Olsson, M. Rostkowski, J.H. Jensen, Improved Treatment of Ligands and Coupling Effects in Empirical Calculation and Rationalization of pK(a) Values, Journal of Chemical Theory and Computation, 7 (2011) 2284-2295.

[63] G.A. Kaminski, R.A. Friesner, J. Tirado-Rives, W.L. Jorgensen, Evaluation and reparametrization of the OPLS-AA force field for proteins via comparison with accurate quantum chemical calculations on peptides, Journal of Physical Chemistry B, 105 (2001) 6474-6487.

[64] R.A. Friesner, R.B. Murphy, M.P. Repasky, L.L. Frye, J.R. Greenwood, T.A. Halgren, P.C. Sanschagrin, D.T. Mainz, Extra precision glide: Docking and scoring incorporating a model of hydrophobic enclosure for protein-ligand complexes, Journal of Medicinal Chemistry, 49 (2006) 6177-6196.

[65] J.M. Hayes, D.D. Leonidas, Computation as a tool for glycogen phosphorylase inhibitor design, Mini-Rev. Med. Chem., 10 (2010) 1156-1174.

[66] E.H. Fischer, E.G. Krebs, Muscle Phosphorylase-B, Methods in Enzymology, 5 (1962) 369-373.

[67] N.G. Oikonomakos, A.E. Melpidou, L.N. Johnson, Crystallization of pig skeletal phosphorylase b. Purification, physical and catalytic characterization, Biochim Biophys Acta, 832 (1985) 248-256.

[68] S. Saheki, A. Takeda, T. Shimazu, Assay of inorganic phosphate in the mild of pH range, suitable for measurement of glycogen phosphorylase activity, Anal. Biochem., 148 (1985) 277-281.

[69] R.J. Leatherbarrow, GrafFit Version 6.0. Erithakus Software, Staines, UK., in, 2007.

[70] K.M. Alexacou, A.C. Tenchiu Deleanu, E.D. Chrysina, M.D. Charavgi, I.D. Kostas, S.E. Zographos, N.G. Oikonomakos, D.D. Leonidas, The binding of beta-d-glucopyranosyl-thiosemicarbazone derivatives to glycogen phosphorylase: A new class of inhibitors, Bioorg Med Chem, 18 (2010) 7911-7922.

[71] W. Kabsch, Xds, Acta Crystallogr D Biol Crystallogr, 66 (2010) 125-132.

[72] CCP4, The CCP4 suite : programs for protein crystallography, Acta Crystallogr., D 50 (1994) 760-763.

[73] P.R. Evans, G.N. Murshudov, How good are my data and what is the resolution?, Acta Crystallogr D Biol Crystallogr, 69 (2013) 1204-1214.

[74] G.N. Murshudov, P. Skubak, A.A. Lebedev, N.S. Pannu, R.A. Steiner, R.A. Nicholls, M.D. Winn, F. Long, A.A. Vagin, REFMAC5 for the refinement of macromolecular crystal structures, Acta Crystallogr D Biol Crystallogr, 67 (2011) 355-367.

[75] A.A. Lebedev, P. Young, M.N. Isupov, O.V. Moroz, A.A. Vagin, G.N. Murshudov, JLigand: a graphical tool for the CCP4 template-restraint library, Acta Crystallogr D Biol Crystallogr, 68 (2012) 431-440.

[76] R.P. Joosten, F. Long, G.N. Murshudov, A. Perrakis, The PDB_REDO server for macromolecular structure model optimization, Iucrj, 1 (2014) 213-220.

[77] V.B. Chen, W.B. Arendall, 3rd, J.J. Headd, D.A. Keedy, R.M. Immormino, G.J. Kapral, L.W. Murray, J.S. Richardson, D.C. Richardson, MolProbity: all-atom structure validation for macromolecular crystallography, Acta Crystallogr D Biol Crystallogr, 66 (2010) 12-21.

[78] M.D. Winn, C.C. Ballard, K.D. Cowtan, E.J. Dodson, P. Emsley, P.R. Evans, R.M. Keegan, E.B. Krissinel, A.G. Leslie, A. McCoy, S.J. McNicholas, G.N. Murshudov, N.S. Pannu, E.A. Potterton, H.R. Powell, R.J. Read, A. Vagin, K.S. Wilson, Overview of the CCP4 suite and current developments, Acta Crystallogr D Biol Crystallogr, 67 (2011) 235-242.

[79] S. McNicholas, E. Potterton, K.S. Wilson, M.E. Noble, Presenting your structures: the CCP4mg molecular-graphics software, Acta Crystallogr D Biol Crystallogr, 67 (2011) 386-394.

Highlights:

- C-(β-D-glucopyranosyl)-1,2,4-triazoles as inhibitors of glycogen phosphorylase
- QM/MM docking employed as an effective tool for virtual screening
- New synthetic method for the title compounds
- X-ray crystallography has revealed interactions favorable for potency
- Compounds demonstrate promising predicted pharmacokinetic profiles